Prestress and adhesion site dynamics control cell sensitivity to extracellular stiffness

S. Féréol[*], R. Fodil[*], V.M. Laurent[*], M. Balland[§], B. Louis[*], G. Pelle[*♣], S. Hénon[§], E. Planus[*], and D. Isabey[*]

[*] 1. Inserm UMR 955, IMRB, Biomécanique Cellulaire et Respiratoire, Créteil, F-94000, France
2. Université Paris 12 Val-de-Marne, Faculté de Médecine, Créteil, F-94000, France

[♣] AP-HP, Hôpital Henri Mondor, Service de Physiologie - Explorations Fonctionnelles, Créteil, F-94010 France

[§] 1. CNRS UMR 7057, MSC, Physique du Vivant, Bât. Condorcet, Paris, F-75013, France
2. Université Paris 7 - Denis Diderot, UFR Physique, Bât. Condorcet, Paris, F-75013, France

Correspondence address:

Daniel Isabey
Inserm UMR 955, Equipe Biomécanique Cellulaire et Respiratoire (n°13)
Faculté de Médecine
8, rue du Général Sarrail
94 010 CRETEIL Cedex, France
Phone: 33 1 49 81 37 00
Fax: 33 1 48 98 17 77
E-mail: daniel.isabey@inserm.fr

Running tittle: Extracellular stiffness cell sensitivity

Key Words: Cell mechanosensitivity, Cell mechanics, Force regulation by adhesion sites, Extracellular Environment, Substrate rigidity, Dissociation force.

Abstract

This study aims at improving the understanding of mechanisms responsible for cell sensitivity to extracellular environment. We explain how substrate mechanical properties can modulate the force-regulation of cell sensitive elements primarily adhesion sites. We present a theoretical and experimental comparison between two radically different approaches of the force-regulation of adhesion sites which depends on their either stationary or dynamic behavior. The most classical stationary model fails to predict cell sensitivity to substrate stiffness while the dynamic model predicts extracellular stiffness dependence. This is due to a time-dependent reaction force in response to actomyosin traction force exerted on cell sensitive elements. We purposely used two cellular models, i.e., alveolar epithelial cells (AECs) and alveolar macrophages (AMs) exhibiting respectively stationary and dynamic adhesion sites, and compared their sensitivity to theoretical predictions. Mechanical and structural results show that AECs exhibit significant prestress supported by evident stress fibers and lacks sensitivity to substrate stiffness. On the other hand, AMs exhibit low prestress and exhibit sensitivity to substrate stiffness. Altogether, theory and experiments consistently show that adhesion site dynamics and cytoskeleton prestress control cell sensitivity to ECE with an optimal sensitivity expected in the intermediate range.

INTRODUCTION

Cell sensitivity to Extracellular Environment (ECE) is fundamental for many biological functions such as cell-tissue interactions, cell migration, tissue repair, differentiation (1-4). Importantly, an ECE-dependent regulation of the cell response to intra/extracellular forces raises a number of fundamental questions. The latter requires to take into account, in addition to the morphological and mechanical cell behaviour (5, 6), the physics of bond dissociation under force application (7, 8). Surprisingly, the physical mechanisms sustaining the role of substrate relaxation have been largely occluded in the literature. A key assumption to understand these phenomena is that activation of substrate-sensitive cell elements must be mechanically limited by substrate relaxation (9). Based on theoretical equations taking into account protein mechanics, substrate relaxation and traction force, it can be shown (see Appendix) that force-regulation of cell sensitive elements appears to be dependent on two main factors, i.e., adhesion site dynamics and actomyosin-dependent cellular prestress. Importantly, these molecular/cellular factors involve coupling between some specific intracellular or transmembrane proteins and cytoskeleton filaments. It is through these coupling mechanisms that cell sensitivity to substrate stiffness is rendered physically possible and biologically effective.

In spite of the lack of theoretical understanding supporting cellular mechanosensitivity, the role of adhesion sites and cytoskeleton prestress can be suspected from many experimental reports.

Adhesion sites are clusters of transmembrane-associated proteins that link the cytoskeleton (CSK) to ECE. In response to mechanical stimuli, adhesion sites can maturate through a force-dependent molecular reinforcement (10). Hence, the capacity of adhesion sites to transmit forces to ECE. For instance, Initial Adhesion IA can support forces in the pN range (11), Focal Complex (FC) support forces in the nN range (12). Forces supported by Focal Adhesions (FA) may reach higher values, let say up to 100 nN (13). An additional key difference is that IAs and FCs are mostly dynamic adhesion sites, i.e., life times vary from a few seconds to 10-20 min while focal adhesion lifetime is about 30–90 min (14). Noteworthy, with rupture forces in the range 40-60 pN (15) and a life time from 2 to 12 min (16), Adhesion Complexes such as Podosome Type Adhesion (PTA) rather belong to dynamic adhesion sites. Note that podosome lifespan tend to decrease as substrate flexibility decreases (17). The present study provides experimental and theoretical arguments showing that, depending on their either stationary or dynamic behavior, opposite responses can be expected in terms of force regulation by tissue rigidity.

Cellular prestress has an evident structural origin residing through tensed actinic CSK elements which are cross-linked with contractile intracellular proteins of the myosin type, resulting in intracellular tension and contraction (18-20). Acto-myosin contraction is also responsible for pulling actin filaments, and generating actin retrograde motion (21). CSK prestress has been linked to the activation level of contractile apparatus (22). The CSK prestress dependence on cell sensitivity to ECE is consistent with previous conclusions about the key role of cytoskeletal prestress for mechanotransduction (23). However, the present concept of cell sensitivity is fundamentally different from earlier concepts such as the one proposed by Chiquet et al., which is based on static force equilibrium between cell and substrate. Indeed, we consider that cells sense mechanical properties of ECE in the early phase of protein-ECE or protein-CSK linkage. This time let for cell sensitivity to be effective is also the time required for maturation of the protein-CSK linkage. Thus, because extracellular properties trigger the development of dynamic adhesion sites, they promote force regulation of adhesion sites by ECE stiffness.

We present a coupled theoretical and experimental study of the comparison between two radically different approaches of the force-regulation of adhesion sites: the classical stationary approach and a rather new dynamic approach of cellular sensitivity to substrate stiffness. Two cellular models were purposely chosen for representing static and dynamic adhesion systems. The FA-representative highly tensed cellular model was provided by alveolar epithelial cells grown at confluence (AECs). The FC-representative slightly tensed cellular model was provided by isolated alveolar macrophages at rest (AMs). Present immunostaining results show that AEC model exhibits a wide majority of stationary fully locked adhesion sites while isolated AMs express dynamic adhesion sites called podosomes as previously reported in the literature (16, 24). Mechanical results show that the two cellular models tested consistently differ in terms of mechanical feature notably CSK-stiffness and prestress. In order to focus on the sole effect of changing mechanical properties of ECE, AMs were chemically non activated, remaining mostly at resting state. Note that the two studied cell types are physiologically interdependent, as they interact mechanically and biologically in the same physiological environment, i.e., pulmonary alveoli (25). In the present study, a mechanically active ECE was created by means of RGD-coated microbeads (~ 4 µm-diameter ferromagnetic or silicate beads) attached to integrin transmembrane mechanoreceptors and moved by either Magnetic Twisting Cytometry (MTC) or Optical Tweezers (OT) (see Material and Methods). Mechanically passive ECE was created by soft and stiff polyacrylamide gels and rigid glass/plastic substrates. Noteworthy, experimental results confirm the validity of theoretical predictions. A predictive and synthetic diagram is proposed. It enlightens the role played by adhesion site dynamics and CSK prestress in the cell sensitivity to ECE stiffness.

MATERIAL AND METHODS

Type I collagen coating of glass and plastic substrate

Concentrated stocks of type I collagen (BD Biosciences) were diluted to 20 µg/ml in 0.02 N glacial acetic acid. The diluted proteins were dispensed into 96-well culture plates 8-well LAB-TEK chambered coverglass and on glass coverslips and 22 mm×22 mm glass coverslips and were incubated for 3 hours at room temperature. Coated wells were routinely washed 3 times with sterile water, dried and kept at 4°C.

Preparation of polyacrylamide gels and coating with type I collagen

Polyacrylamide gels were prepared according to a method previously described in (26) using 10% of acrylamide and 0.3 % (for soft gel) or 0.07% (for rigid gel) bis-acrylamide. Atomic Force Microscope (NANOWIZARD, JPK Instruments, Berlin, Germany) indentation was performed to confirm that the elasticity modulus of the gels was close to expected values, i.e., 58 kPa for 0.3% bis-acrylamide and 23 kPa for 0.07% bis-acrylamide (6). Values of softer gels are close to the optimal values found by Solon et al. for maximum spreading of fibroblasts (27). Gels were coated with 200 µg/ml type I collagen solution (26).

Cell isolation, culture preparation and bead attachment

AMs were isolated from Sprague-Dawley rats by broncho-alveolar lavages and re-suspended in RPMI medium supplemented with 0.1% BSA, and plated at a density of 10^6 cells/ml for 3 hours on the various type I collagen-coated substrates studied: 96-wells culture plates, glass coverslips, Lab-Tek chambered coverglass (8-wells) and polyacrylamide gels, as described in (6).

A549 human AECs (American Type Culture Collection, Rockville, MD) were grown under the conditions described in (25), on the same substrates as those used for AMs. Their density was adjusted to obtain confluence at 24 hours.

Before bead attachment to cells, AMs and AECs were incubated in serum free culture medium (RPMI 1640 for AMs and DMEM for AECs) supplemented with 0.1% BSA for at least 30 minutes at 37°C to block non-specific binding. Beads were then added to the cells at a dose of 40 mg per well (96-well plates), or 100 mg per coverslip for 30 min at 37°C in a 5% CO_2 and 95% air incubator. Unbound beads were washed away 3 times with serum-free culture medium-1% BSA.

Carboxyl ferromagnetic beads (Spherotech Inc. (Brussels, Belgium)) or carboxylated silica beads (Bangs Laboratories Inc. (USA)) of similar sizes (4.5 µm and 3.5 µm in diameter respectively) were coated with the same RGD peptide (PepTite-2000, Telios Pharmaceuticals Inc. (San Diego, CA, USA)), as described in (28).

Magnetic Twisting Cytometry (MTC)

Cell elasticity modulus was assessed by an MTC device (MTC) initially described by Wang et al. (29) and improved by our group to take specific geometrical factors into account (6, 28, 30). In the case of gel substrates, cells were grown at confluence to obtain exclusive bead attachment to the cells.

It should be noted that, under these experimental conditions, most AMs were resting despite of the local stimuli applied by the beads. Moreover, the minority of AMs with high rigidity (e.g., migrating AMs) did not contribute to the averaged cell stiffness measured by MTC, as the MTC averaging procedure attributes a higher weight to beads experiencing large rotations (see (30)).

To quantify cellular prestress (31), the effect of actin depolymerization on cell stiffness was studied by treating AMs and AECs with low concentrations of cytochalasin D (1 µg/ml) and performing MTC measurements at different times (3, 6 and 11 min).

Optical Tweezers (OT)

The cell elasticity modulus of AMs adherent to the gel substrate was assessed by Optical Tweezers (OT) using a previously described device (32). An RGD-coated silicate bead attached to a cell was trapped in the tweezers. The trap was then displaced at a low constant speed of ~0.1 mm.s^{-1}, i.e., under almost quasi-static conditions and in a direction parallel to the coverslip and the cell membrane. The range of forces applied (0.1–200 pN ensured that cellular deformations remained in the low range (< 500 nm) (28). The CSK elastic modulus was determined after appropriate correction for geometric factors estimated bead by bead from the recorded microscopic images (28, 30).

F-Actin and paxillin staining and 3D CSK rendering

After 3 hours for adherent AMs and 24 hours for AECs, F-actin and paxillin staining was performed after fixation in paraformaldehyde (4% in phosphate buffer pH 7.4) for 10 min, then fixed cells were incubated with mouse antibody against paxillin (BD Bioscience, France) and rhodamine phalloidin (Sigma Chemicals, l'Ile d'Abeau Chêne, France) for 45 min at 37°C. After washes, cells were incubated with Alexa 488 goat antimouse antibody for 45 min at 37°C. After final wash, cells were then covered with mounting medium and stored at 4°C overnight before observation by laser confocal microscopy (28).

Stained cell monolayers were observed using the Pascal 5 confocal microscope (Zeiss, Rueil-Malmaison, France). Image processing was performed using AMIRA software (Version 4.1.2., Visage Imaging, Carlsbad, CA USA). Fields of cells were randomly selected and brought into focus using ×63/1.4 numeric aperture Plan Neofluor objective. Optical cross-sections were recorded at 0.3-µm z-axis intervals to reveal intracellular fluorescence. Before 3D-visualization, using theoretical PSF, stack of gray-level images (8 bits) was subjected to deconvolution. 3D-visualization was performed using AMIRA software.

3D-reconstruction and rendering of CSK structure was performed by AMIRA software using gray-level images of each confocal z-stack. 3D-skeletonization of the dense polymerized CSK structure was performed using the Skeleton pack of AMIRA software.

Simulation methods

We compared, for quasi static conditions, the stress fields induced at the cell-substrate interface (i.e., the 3D-tensions virtually "seen" by adhesion sites on both the intracellular and the extracellular sides) while tested substrate Young modulus may differ by several orders of magnitude. We purposely used a numerical model previously developed to describe mechanical interactions between bead, cell and substrate (6, 30). In this idealized model, cell and substrate are homogeneous quasi-incompressible and hyperelastic (neo-Hookean) continuum characterized by a classical strain energy function already used in tissues and living cells (33) and given by $W = a_1(I_1 - 3)$ where a_1 is the cell constant (in Pa), while I_1 is the first invariant of the right Cauchy–Green strain tensor C [$I_1 = \mathrm{Trace}(C)$]. In this model, the traction applied by the cell to the different substrates is induced by a bead partially immersed in the cell and through which a constant torque is applied. The cell Young modulus is fixed at a constant physiologically-relevant value of 100 Pa. We assumed no-slip boundary conditions at the bead-cell interface and at the cell-substrate interface. The substrate was attached to a non-deformable base. The bead surface was modeled as a rigid shell whose stiffness is far larger than the cell stiffness. Simulations were performed under static conditions. Computations of the stress fields corresponding to torques 750 pN × µm were performed using a resolution method described in a previous paper (30).

RESULTS

Experimental evidence of the distinct features of AECs and AMs

- Actin CSK-structure and adhesion protein localization

After fixation and double staining of F-actin and paxillin (see Material and Methods), AECs and AMs adhering on the same type I collagen-coated glass substrates were compared for their F-actin organization and the localisation of typical adhesion protein near the basal plane. To do so, we used a cumulative view made of z-stack images within a 1µm-thick layer from the basal cell plane (Fig. 1a-f). Actin and paxillin are representative of the physical link existing between F-actin CSK and ECE. These cellular elements are present at the cell-substrate interface in the two cellular models used (Fig. 1a,b). Such a result was expected as focal adhesion and podosome both contain actin and paxillin (14, 24, 34). 3D-skeletonization of F-actin structure in AECs (Fig. 1c) and in AMs (Fig. 1d) reveals marked differences in the dense CSK architecture (in white) between AECs and AMs. In Fig 1 c-f, the horizontal (c, d) and vertical (e, f) distribution of paxillin is shown by a spatial reconstruction which evidences its aggregation. Marked differences exist in the horizontal distribution of paxillin between the two cellular models used. In AECs, the dense F-actin network near the basal plane covers the entire cell due to multiple interconnections between short and long dense actin stress fibers (Fig. 1c). The later are generally terminated by focal adhesion plaques (visible through reconstructed aggregates of paxillin, in green) notably located on cell periphery in AECs. In AMs (Fig. 1d), the dense F-actin network does not extend throughout the entire cell, forming either punctuated structured or only local network, except at the origin of the circumferential lamellipodium. The presence of a highly structured actin network at the cell edge of AECs and further inside the cell is consistent with the assumption of cellular stability for this type of tissue cell grown to form a monolayer. Punctuate structures of dense F-actin essentially found near basal face of AM body are not commonly observed although this is consistent with the finding that AMs adhere to their substrate through localized and dense actin core developing vertically. These actin structures are usually surrounded by a diffuse membrane domain of integrins and associated proteins such as paxillin forming adhesion complex of the podosome type (14, 24, 35).

- Mechanical response to increasing externally applied stress.

The responses of: (i) AECs (forming a confluent monolayer) and (ii) AMs (essentially resting) to increasing magnetic torques applied through RGD-coated beads (see Material and Methods), were compared over about a minute of stress application, in adherent cells on type I collagen-coated plastic substrate. The short-term cellular response expressed in terms of CSK elastic modulus (Fig. 2) and cellular deformation (Fig. 3) were evaluated at four increasing levels of magnetic torques ranging from 400 to 1300 pN·µm. The results show that resting AMs are clearly softer than AECs, and that AMs and AECs exhibit a markedly different behavior in the short-term response to increasing levels of externally applied stress. AECs exhibit a highly significant stress-dependent increase in cell stiffness (almost linear stress-hardening as shown in Fig. 2) corresponding to non-linear torque-rotation relationship (shown in Fig. 3). In contrast, AMs exhibit a stress-independent cell stiffness throughout the entire range of torque tested (shown in Fig. 2), i.e., quasi-linear stress-strain relationship (shown in Fig. 3). Considering the intermediate to large range of cellular deformation measured, (i.e., 20°-50° of bead rotation corresponding to 900-2100 nm of circumferential bead displacement shown in Fig. 3), it is reasonable to consider that the response of cells structured with stress fibers such as AECs reflect higher geometric non-linearity than cells lacking stress fibers such as AMs.

- Mechanical response to decrease in internal tension.

AECs and AMs exhibited a different response following treatment with low concentrations of cytochalasin D (see Material and Methods, and Fig. 4). While the elastic modulus of AMs remained unchanged for 12 min after blockade of actin polymerization (i.e., from time zero in Fig. 4), AECs exhibit a rapid and significant decrease in elastic modulus after only 6 min of cytochalasin D treatment. The fall in cell stiffness reaches 35% at 11 min. The rapid drop in cell stiffness observed is given to reflect the specific actinic contribution to cell stiffness which can be related to the level of cellular prestress (31, 36). At the low concentration and short duration of treatment used, cytochalasin D mainly affects the deep and dense actin CSK (e.g., stress fibers in AECs) and only minimally cell shape at least in living AECs (37). This cellular response to a decrease in internal stress caused by cytochalasin D reveals the significant level of prestress in AECs compared to the non-measurable level of prestress in AMs. Incidentally, if tension in the actomyosin network is considered to be determinant for stress fiber formation (38), it seems logical that low stressed cells such as AMs lack actin bundles, and subsequently not exhibit a structural non-linear behavior with increasing stress. It should be underlined also that the bead twisting method presently used allows an estimate of cell prestress in non contractile cells. This method does not necessarily reflect the very local intracellular tensions distant from the bead, (e.g., those generated by punctual adhesion structures in the basal plane).

Experimental evidence of the distinct substrate stiffness sensitivity of AECs and AMs

The long-term responses of the two cellular models to type I collagen-coated substrates with three different levels of stiffness are compared in Fig. 5. Cells were allowed to adhere to these substrates for 24 hours for AECs and 3 hours for AMs. The three substrates tested were: (i) rigid substrate made of plastic (for MTC measurements) or glass (for OT measurements) (i.e., Young modulus, $E_s \geq 3$ MPa), (ii) stiff polyacrylamide gel substrate (i.e., $E_s \approx 58$ kPa) and (iii) soft polyacrylamide gel substrate (i.e., $E_s \approx 23$ kPa).

3D-visualizations of F-actin structures (Fig. 5A1 to A6 for AECs and Fig. 5B1 to B6 for AMs) confirm the differences at the cellular level between F-actin structures of AECs and AMs, as already shown in Fig.1. Another important message provided by these actin structure visualizations shown in Fig.5 was that very different substrate stiffness did not affect the stress fiber organization or shape of AECs, e.g., the maximal height of the AEC monolayer remained close to 8-10 µm for all substrates tested. The lack of sensitivity of AECs to substrate properties is confirmed by MTC measurements of AEC elastic modulus showing that AEC stiffness is not affected by the marked changes in substrate rigidity (Fig. 5A bottom graph). In contrast, AM shapes appear to differ according to the substrate: Images B3 to B1 illustrate the slight but significant increase in basal area of AMs while images B6 to B4 illustrate the decrease in cell height observed with increasing substrate rigidity from soft gel to rigid glass. This AM sensitivity to substrate stiffness is confirmed by the significant increase in AM elastic modulus observed when substrate stiffness changed from soft gel to rigid glass (Fig. 5B Bottom graph).

Another interesting feature of actin structures (shown in Fig. 5 A and B) concerns the differences in cell internal tension between the two cellular models studied. Internal tension in AECs can be estimated from the centripetal curvature that characterizes most of the long actin stress-fibers which are tensed between anchorage points to the substrate, i.e., typically the stationary focal adhesion (FA) plaques located at the end of stress-fibers. Such tensed stress-fibers do not exist in AMs, consistently with the lack of prestress measured by MTC.

Theoretical prediction of the distinct substrate stiffness sensitivity of AECs and AMs

- <u>Quasi-static simulations of the stress field at the cell-substrate interface</u>

We used a numerical model of the bead-cell-substrate mechanical interactions to validate in 3D the assumption that reaction forces exerted by the substrate on a stationary adhesion site could not depend on substrate rigidity. In such a case, a constant torque is applied to the bead and generates a three-dimensional stress field extending down to the cell-substrate interface, the higher the torque and/or the stiffer the substrate, the deeper the stress propagation inside the substrate. To verify that substrate stiffness does not affect the 3D-stress field at given torque, we numerically simulated the effect of a constant torque (i.e., 750 pN×µm in simulations) applied to a cell of predetermined and constant elastic properties (i.e., Young modulus of cell fixed at 100 Pa), adhering on three different substrates tested (i.e., Young modulus of 3×10^6 Pa for plastic, 58×10^3 Pa for stiff gel and 23×10^3 Pa for soft gels). The simulated stress fields shown in Fig. 6 are the strictly the same despite profound changes in substrate elasticity properties. Thus, intracellular stress fields, here generated by a twisted bead, could not be affected by substrate stiffness. These results confirm that adhesion sites located at cell-substrate interface could only see the same stress field in spite of deep change in substrate stiffness. Thus, the reaction forces exerted by the substrate on a stationary adhesion site and its force sensitive proteins could not be dependent on substrate rigidity. It strongly suggests that activation of stationary adhesion site containing force-sensitive proteins cannot be regulated by substrate rigidity.

- <u>Comparison between stationary and dynamic cell-substrate adhesion</u>

The predicted behavior of dynamic adhesion sites is presented in Fig. 7 in terms of the relationship between normalized dissociation force and substrate stiffness (see Appendix). In the dynamic adhesion model, once the filament bundles "locks" the adhesion site, retrograde motion of the filament vanishes and the full traction force T is applied to the adhesion site. According to the model, there is no possibility to return to the logarithmic lower branch. AECs monolayer correspond to the upper branch of the graph (S range: (0 – 1) where adhesion sites are fully locked and behave independently on substrate stiffness. In contrast, AMs correspond to the intermediate branch of the graph in Fig. 7, i.e., the zone of the graph corresponding to substrate-dependent adhesion site reinforcement. Noteworthy, in this zone, an increase in substrate stiffness can promote reinforcement simply because the rate of increase of the reaction force $F_{ex}(t)$ (= $k\ V_R$ t) in Eq. A4 increases. In such a case, the time to reach the level where the site locks is shorter. Note that excessively soft substrates correspond to lowest rates of increase in reaction force and adhesion sites lose the possibility to reach the critical force level F_c (S=0) for locking. Note also that for immature adhesion sites such as S~-1, the level of dissociation energy is so low that the adhesion sites have no chance to reinforce, i.e., a stiffened substrate is not sufficient. In these conditions, the adhesion site would remain always immature, and therefore fully slipping.

DISCUSSION

The present paper proposes a new understanding of cellular sensitivity to substrate stiffness. We purposely used complementary theoretical and experimental approaches of this well-recognized but not fully understood phenomena. Based on this coupled approach, we compare two radically different theories of the force-regulation mechanism namely a classical theory describing stationary adhesion sites and a newly proposed theory describing dynamic adhesion sites. It is noteworthy that the most classical stationary model fails to predict cell sensitivity to substrate stiffness while the newly proposed dynamic model provides a rationale to this mostly obscure phenomenon. These two models are thoroughly discussed and confronted with experimental results. The two cellular models used for this confrontion are (i) alveolar epithelial cells (AECs) and (ii) alveolar macrophages (AMs) which exhibit respectively stationary and dynamic adhesion sites. An important finding of this study is the consistency between experimental results and theoretical predictions, namely the cellular model with stationary adhesion site and high internal tension does not exhibit sensitivity to ECE stiffness while the cellular model with dynamic adhesion sites and low or moderate internal tension exhibits sensitivity to ECE stiffness. Because testing adhesion sites isolated from their intra/extracellular environments has no meaning, we tested the sensitivity of cellular models chosen for their capability to represent these two different states of adhesion and intracellular prestress. An important message brought by the dynamic model is that cellular sensitivity to substrate stiffness is possible because, in response to actomyosin traction forces exerted on initial cell sensitive element, a time-dependent reaction force grows with time and, remarkably, remains proportional to substrate elasticity and intracellular tension.

In terms of cell sensitivity to substrate stiffness, experiments and theory reveal the role of two important parameters, e.g., adhesion site dynamics and cytoskeleton prestress. These two parameters enlighten the close connection existing between molecular and cellular mechanisms for the control of cell sensitivity to substrate stiffness. Indeed, the role of adhesion dynamics results from molecular considerations issued from the stochastic processes of bond rupture usually characterized by single molecule force spectroscopy experiments (8, 39-41). The role of intracellular tension results from cellular considerations after assessment of the actinic contribution to cytoskeleton mechanics (42-44). The recent model of force regulation by nascent adhesion sites proposed by Bruinsma (9) provides further support to earlier protein mechanic models, which all predict a dissociation force which is logarithmically dependent on the loading rate (8). Note that protein mechanic models usually consider a reversible chemomechanical activation of adhesion proteins, i.e., between a passive and an active state which is related to conformational change of integrins (7, 45). Importantly, in the dynamic adhesion site model, because the equilibration time for site activation is due to mechanical relaxation and not to chemical equilibration, mechanical relaxation is a factor permitting - thus controlling - cell sensitivity to substrate stiffness. The dynamic adhesion site model also assumes that the actin bundle - to which the adhesion site is connected via a potential energy - is exposed to a constant effort resulting from constant activation of intracellular motors responsible for internal tension or contractility. The important feature of the dynamic adhesion site model (governed by Eq. A4 given in Appendix) is that - in response to an imposed constant actomyosin loading force - a time-dependent reaction force exists and raises with time, allowing the adhesion site to initiate its maturation, i.e., developing towards either site reinforcement or bond rupture. The rate at which the reaction force increases depends on substrate elasticity and acto-myosin motors activation level through respectively the k and V_R term dependence of the slope of the time-dependent reaction force. These predictions are consistent with current biological experiments showing that the issue of adhesion site development, i.e., toward either site maturation or bond rupture, depends extracellular and intracellular conditions. It can be said that a faster rate of increase in the reaction force $F_{ex}(t)$ results in a faster linkage of adhesion site or otherwise, in a higher number of binding-dissociation-rebinding cycles which may in turns favour adhesion site reinforcement. Comparing this dynamic adhesion site model to a stationary adhesion site model, it appears that the behaviors of these two models is completely different in terms of substrate-dependence of force regulation. In response to intracellular traction (internal tension or contraction), the nanoscale motion of the dynamic adhesion site is governed in the early phase of its development by the elasticity of the substrate and intracellular traction force. Note that the higher intracellular traction force, the higher intracellular prestress, the higher the reaction force. It seems also reasonable to consider that substrate stiffness-dependent cellular sensitivity could be favoured by rapid and thus non-distant transmission of intracellular forces, a typical configuration encountered in podosome-like structures of AMs (35) and not in focal adhesion structures of AECs.

We are aware that the results (Fig. 5) only provide a “time-integrated” view, i.e., over several hours. This time is much longer than the mechanical relaxation time associated to adhesion site maturation, τ (= γ_R/k), i.e., about 0.1 s per actin filament which gives relaxation time in the range 10-10^2 s for an actin bundle, letting plenty of time for adhesion site development. On the other hand, the mechanical relaxation time is much longer than the time required for chemical equilibration which is consistent with the above mentioned assumption that the rate-limiting step for activation is mechanical and not chemical. Moreover, due to the lack of knowledge about the dynamics of proteins unfolding and the uncertainty on molecular organization (e.g., cooperative bonds acting in parallel or non-cooperative bonds acting in series), it is presently difficult to accurately estimate the values of critical substrate stiffness $\tilde{k}_c$ and reference value of substrate stiffness k_0 proper ro each substrate (see Fig. 7 and Appendix). Hence, the difficulty to quantitatively estimate the dissociation forces associated to the different conditions tested.

Predictive Diagram

The experimental and theoretical results can be presented schematically in a synthetic diagram (Fig. 8). This diagram predicts cell sensitivity to substrate stiffness as a function of the two main parameters imposed by both theoretical considerations and experimental results: (i) state or strength of adhesion sites, and (ii) CSK prestress or alternatively contractility generated by actomyosin motors. The biphasic shape of this diagram represents the recent knowledge acquired from both experimental results and the theoretical models presented in Appendix. It shows that cell sensitivity to substrate stiffness is optimal for an intermediate range of the mechanobiological parameters. It requires dynamic but locked adhesion sites and intermediate CSK prestress or moderate actomyosin activation. It means that the sensitivity of cellular elements that arises from coupling between specific mechanosensitive proteins (e.g., adhesion proteins) can only be optimal for a certain range of functioning. This is consistent with recent findings concerning the two phases - bell shaped - cellular models predicting that substrate stiffness influences many cellular processus such as spreading or traction forces. These models may be thermodynamics (46), kinetic (47) or even purely mechanical (48). Note that substrate stiffness has been thought to be a more important determinant for cell shape than the density of adhesive ligands to which the cell binds (46).

The first horizontal axis (strength of adhesion sites) represents the maximum force supported by a given adhesive link, (i.e., represented by $\tilde{F}(\tilde{k})$ in Appendix). This strength depends on the adhesion site molecular structure and the content of the adhesion site. The simplest link in terms of molecular adhesion structure corresponds to Initial Adhesion (IA). IA can support forces in the pN range (49) and slips at higher forces - a phenomenon called “slipping clutch” - but preventing adhesion linkage at higher forces. For totally slipping adhesion sites (i.e., $S \sim -1$, see Appendix), the force regulation by substrate stiffness may not be effective as the site dissociates before binding. If IA matures to FC, over an interval of about one minute, the link with CSK would be reinforced due to a larger number of constituent components such as vinculin or paxillin. Therefore, the adhesion structure would be able to support forces in the nN range (12). The clutch has engaged which is is well described by the degenerate free energy condition $S \sim 0$ (see Appendix). In this range of intermediate strength, i.e., for FC adhesion site structure, the dynamic adhesion site theory described in the Appendix predicts force regulation by substrate stiffness, hence the prediction of maximum sensitivity given by the diagram. The FA structure can support forces approaching 100 nN, i.e., close to the μN range (50). FA take much longer to achieve this molecular reinforcement, FA require much more time than FC to become fully established (about one hour) (51). Although fully mature adhesion sites (FA) remain important centers for cell signaling by reversibly adjusting their size to the applied force (52), they remain insensitive to substrate stiffness for the theoretical reasons explained in the first part of the Appendix.

The second horizontal axis of the diagram represents prestress, which corresponds to the level of endogenous contractile tension in the CSK generated by actin-myosin II interactions. It is well represented by the traction force applied to actin bundle (called T in Appendix). Based on the present experimental results, we consider that the prestress level differs according to local or distant generation of actomyosin motors. Podosomes can only generate a local prestress - not measurable by bead twisting from the apical side of AMs. By contrast stress-fibers can propagate the tensile prestress over long distances throughout the cell structure (53), contributing to the elevated prestress measured in AECs. Note that prestress in highly contractile cells has been shown to remain proportional to cellular stiffness (42).

The level of endogenous contractile prestress generated by actomyosin contraction is known to play a key role in the cellular adaptation to stress (54)(18). The use of myosin II inhibitors such as blebbistatin has provided additional evidence that actomyosin activity plays a key role in the cellular adaptation to an externally applied mechanical stress (55).

Incidentally, this active adaptation may be seen as complementary to the structural, essentially passive, cellular adaptation. Non linear and passive behaviour of highly prestressed and largely deformed cellular structures is well described by the tensegrity model (22, 29, 56).

It is now recognized that maturation and strengthening of adhesions sites are dependent on internal CSK forces and/or extracellular stimuli (10, 12, 57). Moreover, the role of actomyosin contractility on maturation of adhesion sites has been demonstrated by using actomyosin inhibitors (57, 58). Similarly, it has recently been shown that mechanical reinforcement - one of the key response of the cell to locally applied stress - is synonymous of actin recruitment and higher actomyosin contraction (59). If we consider that substrate stiffness also regulates actomyosin contraction and thus endogenous tension, one may expect higher reaction force and, for sufficient substrate stiffness, enhanced reinforcement and faster maturation of the adhesion site. Moreover, the assembly of stress fibers and focal adhesion is known since a long time to be regulated by the small GTPase Rho (60). Besser and Schwarz (61) have made a mechanochemical model of the stress fiber reinforcement and increase in contractility induced by the Rho pathway. The model describes the biochemical process of Rho diffusion throughout the cytoplasm, the viscoelastic properties of a stress fiber tensed between two focal adhesion sites and the variable contractile properties of the stress fiber under the variable Rho concentration. Although providing a coupled view of biochemistry and mechanics in the control of stress fiber contraction, this model does not account for the initial reinforcement of adhesion sites and thus could not describe the cellular sensitivity to substrate stiffness. Moreover, it is known that in cells which do not express stress fibers and focal adhesion system such as macrophages, Rho does not directly regulate actin cytosleleton and focal complex adhesion system (62) and is not required for migration (63).

AECs forming a monolayer occupy a low sensitivity zone located in the basal part of the diagram (Fig. 8) where prestress and strength linkage to ECE are both significant. This lack of substrate sensitivity of AECs forming a monolayer is thought to be representative of other tissue cells, which would therefore be situated in the same region of the diagram. For instance, Yeung et al. found similar results in a confluent monolayer of endothelial cells - evidenced by maintenance of a constant cell area - despite very different substrate stiffness (5). We can consider from present results that subconfluent and confluent cells do not totally diverge in terms of structure, shape, mechanics meaning that the subconfluent or confluent character does not affect the present sensitivity results. First, the subconfluent cells structures shown in Fig. 5A 1-6 do not appear significantly modified by substrate stiffness. Second, we earlier performed measurements of CSK stiffness in subconfluent and confluent A549 cells (31) and found no difference in CSK stiffness, stiffening response and prestress. These past and present results are totally consistent with the earlier results obtained in fibroblasts by Yeung et al. who found that, as soon as tissue cells are able to make cell-cell contacts, they form stress fibers even when there are grown on soft substrates (5). These authors also noticed that endothelial cells behave in a similar fashion; precisely they need to be sparse enough and noteworthy lack cell-cell junctions to recover a stiffness-dependent morphology and structure. To explain their results, Yeung at al. assumed that cell-cell adherent junctions formed between endothelial cells involve cadherin activation which could override the ligand-activated integrin signal. We propose a physically-founded explanation for the lack of AECs sensitivity. Based on paxillin staining in AEC model which shows that cell-matrix adhesion maintains the anchorage of the monolayer to the substrate (see Fig. 1), it can be said that the significant level of prestress found in AEC monolayer could not be uniquely balanced by cell-cell adhesion. According to the present results, it can be said that stationary adhesion sites of AEC monolayer keep maintaining the stability of AECs monolayer in a substrate-independent manner. In case where AECs would adopt a migrating phenotype and then become isolated they would recover their sensitivity to ECE stiffness (see the more central position of Tissue Cells in Fig. 8) as experimentally shown by Yeung et al. (5). This is because non stationary adhesion sites of tissue cells are regenerated as required for cell migration. Migrating isolated fibroblasts have been shown to express this type of sensitivity to substrate stiffness via migration guided by substrate rigidity, a phenomenon called durotaxis (2).

Resting AMs occupy a central zone in the diagram (Fig. 8) consistent with our experimental results and theoretical predictions. With rupture forces in the range pN-nN (15), life times not exceeding 12 min (16), dynamic adhesion complexes or podosomes of macrophages are close to FC and thus right in the middle of adhesion site strength axis. The reasons why macrophage adhesion sites remain in the dynamic state and do not mature towards stationary adhesion sites is beyond the scope of this paper. The phagocytosis function of macrophages has been shown to most likely require the development of high contractile forces (64). Note that phagocytosing AMs do not lose their sensitivity to extracellular stiffness properties since objects with identical chemical properties but different stiffness are preferentially engulfed when they are stiff (65). Present results on AMs adherent to coated gels as well as previous results on AMs adherent to epithelial cells (6) show that AMs adapt their shape to ECE stiffness while missing stress-fibers. This is surprising as stress-fibers have been thought to be determinant for mechanotransduction in tissue cells (23, 53, 66). These results on AMs therefore raise a number of questions concerning the nature of mechanotransduction pathways in cells like AMs. Indeed, these cells do not have a prestress-mediated force transmission system such as that described by Wang at al. (53). We recently proposed that microtubules which terminate at podosomes (16, 24) could play a role in mechanotransduction of AMs (6). Podosomes, as dynamic adhesion structures also myosin II-dependent adherent actin microdomains, are able to provide an ECE dependent cell regulation which might be facilitated by the local generation of contractile forces (17, 35, 67). These short-lived punctuate actin rich adhesion structures are also permitting to AMs to be sensitive to ECE stiffness, most likely generating a local prestress limited to the adhesion site region as suggested by the results of this study. This local contractile activity is consistent with a moderate cellular prestress characteristics of our resting AMs. RGD-coated beads essentially located on the apical surface of the cells cannot measure this local prestress, essentially limited to the adhesion site (PTA) vicinity. Altogether, the results obtained in the two cellular models support the concept that intracellular structure and adhesion site function in coordination at different scales to regulate the cellular response to ECE.

Note that interactions of AMs with other cell types, organic and inorganic materials are essential for many lung functions such as adhesion to alveolar epithelium, particle recognition and selective destruction, which all imply specific and essentially dynamic adhesion sites. In addition, cell-cell interactions of AECs with other alveolar cells and matrix which would rather involve stationary adhesion sites, are essential for alveolar stability. An alteration of either AM or AEC interactions with ECE is responsible for many pathological reactions leading to either fibrogenic, granulomatous, destructive or inflammatory processes.

APPENDIX: Simplified theory of force regulation by adhesion sites

We consider the simplest model made of a discrete adhesion site of constant size “a” (~ $A^{1/2}$, A: area of adhesion site) located at the surface (parallel to x-y plane) of a linearly elastic semi-infinite medium characterized by a substrate Young modulus (E_s) (9). The adhesion site is exposed to active and passive unidirectional forces acting at the interface between the substrate and the cell. The active force, generated by an acto-myosin contraction, is transmitted to the site by an actin bundle and is related to internal tension. Traction force is directed along the x-axis and results in adhesion site along the same x-axis direction. The passive force results from the viscoelastic reaction of the substrate to this active force. Alternatively, internal tensions that promote adhesion site assembly could be replaced by application of external forces (14). The aim of the present Appendix is to enlighten the role of physical parameters governing the substrate-stiffness sensitivity in stationary (part A) and dynamic (part B) adhesion sites, and their relationship with overall cell scale properties.

A. Stationary adhesion site

In its simplest form, the adhesion site can be considered to be in an almost static equilibrium between a traction force (T) transmitted via a bundle of actin filaments and a recoil force generated within the viscoelastic substrate, in response to the traction force. Note that the traction force can be generated either intracellularly by acto-myosin motors or extracellularly by a probe provided it is physically connected to the cytoskeleton, e.g., an RGD-coated bead as in the present study. Regardless of its origin, i.e., intracellular or extracellular, the traction force generates a local stress distribution inside the substrate whose area integral is equal to the traction force (T). According to linear elasticity theory, the three components of the resulting elastic displacement of the substrate are all inversely proportional to the substrate Young modulus (E_s), i.e., the stiffer the substrate, the smaller the displacement at a given applied stress. Displacement (u_0) of the adhesion site center of size “a” is given by $u_0 \approx T/(E_s \cdot a)$ (= $(\sigma_0/E_s) \cdot a$), with σ_0 (=T/A) the spatial average of the applied force T, showing that the substrate acts as a harmonic spring of constant k ($\approx E_s \cdot a$) while u_0 always remains proportional to T. This type of property has been used to deduce the traction force from the displacement field (57). Noteworthy, away from the adhesion site, e.g., at a distance “r” from the adhesion site, substrate stress remains proportional to external stress σ_0, times the square of the a/r ratio, but does not depend on substrate rigidity, i.e., $\sigma_{xx}(x=r,\ y=0,\ z=0) \approx -\sigma_0 \left(\frac{\sigma_p + 2}{2\pi} \right) \left(\frac{a}{r} \right)^2$, with σ_p: Poisson ratio. The reaction forces exerted by the substrate on a stationary adhesion site are therefore independent of substrate rigidity. Hence, the linear elasticity theory suggests that force regulation of stationary adhesion sites can only occur via a reversible change in adhesion site area. Interestingly, it has been shown that focal adhesion areas are approximately proportional to the applied forces (52).

B. Dynamic adhesion site

If not stationary, the adhesion site is dynamic and its nanoscale time-dependent displacement has to be considered. Noteworthy, the force-regulation model proposed by Bruinsma (9) considers the relative displacement, ρ(t), between the actin filament bundle and a linked adhesion site (see Fig. A1). If Z(t) is the absolute position on x-axis at instant t of the filament bundle and X(t) the absolute position of adhesion site in such way that $X(t=0)=Z(t=0)=0$, then the relative adhesion site displacement can be written: $\rho(t) = Z(t)-X(t)$. It is also assumed that dynamic - not fully mature - adhesion sites do maintain their size constant “a” while changing their state as maturation occurs. The filament bundle is exposed to a traction force T directed along x-axis. The adhesion site is exposed to a force F parallel to T which derives from a potential energy of linkage between the adhesion site and the CSK. F can only be a small fraction of the actomyosin traction force T to which the actin bundle is exposed. The state of the adhesion site reversibly varies between an inactivated (or passive) state ($S = -1$) and an activated sate ($S = 1$), thus taking into account an integrin activation induced by phosphatase activity triggered by a force-induced conformational change of adhesion site integrins. This is a specificity of the model proposed by Bruinsma (9) compared to previous molecular bond studies (8, 39-41).

Calling ΔG the Gibbs free energy difference between these two states in the absence of applied force, the thermodynamic work performed by the applied force during such conformational change is Fd*, where d* is the characteristic length scale of the molecular displacement, i.e., in the nm range (8, 39, 41). Under chemical equilibrium conditions, the likelihood value of the site variable S is given by:

$$\langle S \rangle_F = \tanh \frac{1}{k_B T}\left(-\Delta G + Fd^*\right) \qquad \text{(A1)}$$

In the present experiments, the state variable S characterizing AM adhesion sites is assumed to be within the range: (-1 - 0) while for AEC adhesion sites it would be: (0 – 1).

The adhesion site is exposed - on the cellular side - to a force derived from the potential energy U(ρ, S) describing the mechanochemical linkage between actin filaments and the adhesion site. The adhesion site is exposed - on the substrate side - to a recoil force resulting from the viscoelastic reaction of the substrate. The latter is made of the viscous drag $\gamma_B \frac{dX}{dt}$ proportional to friction coefficient $\gamma_B\left(\approx \eta\, a\right)$ added to the recoil force $-kX$ proportional to the spring constant k ($\approx E_s$ a) where “a” is the unchanged size of the - not fully mature - adhesion site. $f(t)$ is the thermal random noise exerted on the site provided by Fluctuation-Dissipation theorem. Then, the equation of motion of the site is given by:

$$\gamma_B \frac{dX}{dt} + kX = \frac{dU(\rho, S)}{d\rho} + f(t) \qquad \text{(A2)}$$

The equation of motion of actin filament bundle is obtained by setting the equilibrium between the sum of forces exerted on the bundle - on cellular side - (constant traction force (T), the link force, the thermal fluctuation random force $f^*(t)$ and the viscous retarding force, $\gamma_R \frac{dZ}{dt}$, resulting from the friction between actin filaments and the cytoplasm (friction coefficient: γ_R).

$$\gamma_R \frac{dZ}{dt} = \frac{dU(\rho, S)}{d\rho} + T + f^*(t) \qquad \text{(A3)}$$

T (= $\gamma_R \cdot V_R$) is responsible for the retrograde motion of the actin bundle at the constant velocity V_R.

Combining equations of motion for adhesion site (Eq A2) and of actin filament bundle (Eq A3) and assuming times much shorter than the mechanical relaxation time, i.e., $t \ll \tau = (\gamma_B + \gamma_R)/k$ (= γ_R/k because ($\gamma_B \ll \gamma_R$, a condition indeed verified by the values given above for polyacrylamide gels), the relative motion of the adhesion site of coordinate ρ(t) can be described by a Langevin equation:

$$\gamma_B \frac{d\rho}{dt} + k(\rho - V_R\, t) \cong -\frac{dU(\rho, S)}{d\rho} + \gamma_B V_R + f(t) \qquad \text{(A4)}$$

Eq. A4 describes the nanoscale motion a particle of coordinate ρ(t) moving in a double-well link potential U(ρ, S), subjected to the constant traction force $\gamma_B V_R$ and a time-dependent reaction force $F_{ex}(t)$ (= $k\, V_R\, t$), despite the assumption of constant traction force.

For 1µm-wide site and the three substrates tested in this study (plastic, “stiff” gel, “soft” gel), the spring constant is: k = 3000 pN/nm, 58 pN/nm and 23 pN/nm respectively. Corresponding values of γ_B for the polyacrylamide gels tested remain within the range: $3.\ 10^{-1}$- 3.10^{-4} pN·s/nm (C. Verdier, personal communication). γ_R is of the order of 0.1 pN·s/nm per filament, i.e., 10-100 pN·s/nm for 10^2-10^3 filament per actin bundle. Thus $\gamma_B << \gamma_R$ is a condition indeed verified by the values given above for polyacrylamide gels. V_R is in the µm/mn and characterizes actin dynamics in the lamellipodia. Values of $k\ V_R$ were 48000 pN/s, 928 pN/s and 368 pN/s for the three substrates tested.

Eq. A4 shows that, as filaments drag the adhesion site toward the inner part of the cell, the substrate reaction $F_{ex}(t)$ increases linearly with time: the higher the substrate stiffness, the more rapid the increase in reaction force. At the instant of dissociation, the most likely force exerted on the adhesion site $\langle F(k)\rangle$ exhibits a classical logarithmic dependence on loading rate (8) modulated by the contribution of the activation energy characterizing the adhesion site considered:

$$\frac{\langle F(k)\rangle}{f_\beta} \approx \ln\left\{\frac{k}{J\, f_\beta / V_R}\right\} + \frac{1}{f_\beta}\frac{\langle \Delta \mathrm{U}\rangle}{\rho_f} \tag{A5}$$

with $f_\beta = k_B T / \rho_f$, the single molecule force level for bond dissociation used as a force scale (~13 pN (9)), $k_B T$ is the thermal energy scale (~4pN·nm at biological temperature), ρ_f (~0.3 nm) is the distance at which U(ρ,S) reaches its maximum, i.e., the site dissociates. $k_0\left(= J\, f_\beta / V_R\right)$ represents a stiffness scale which characterizes the dynamic properties of the adhesion site at the molecular level: $J\left[= J_0 \exp\left(-\frac{\Delta \mathrm{U}}{k_B T}\right)\right]$ the attempt rate for escape out of the well or rate of dissociation which depends on (i) local curvature of U(ρ) in the vicinity of dissociation, (ii) friction coefficients and (iii) temperature. For an activation energy of the order of $20k_BT$ corresponding to weak protein-protein links such as a single link activation energy integrin-VCAM, the rate of dissociation J_0 starts at ~10^9-10^{10} Hz and ends at 1 Hz which makes precise quantification of J difficult without additional specific experiments which are beyond the scope of the present study. In Eq. A3, $\langle \Delta \mathrm{U}\rangle$ is the likelihood value of activation energy of the potential during dissociation, or thermal average of the passive (S=–1) and active (S=1) activations energies, i.e.,

$$\langle \Delta \mathrm{U}\rangle = \Delta \mathrm{U} + 1/2\, \Delta\Delta \mathrm{U}\left(1 + \langle \mathrm{S}\rangle_F\right) \tag{A6}$$

with ΔU and ΔΔU the activation energy for escape out of the potential well at (i.e., dissociated adhesion site) at S = -1 and active S = 1 respectively. The logarithmic dependence on substrate rigidity is expected to occur up to a force level F_c corresponding to the threshold rigidity where the energies of the active and passive states degenerate ($F_c=\Delta G/d^*$) and the dissociation force level diverges. For soft substrates, the force loading rate ($k\ V_R$) is low and the site will dissociate from the filaments at a low reaction force level since $\langle F(k)\rangle$ is low (see Eq 3), potentially initiating a succession of binding-dissociation-rebinding cycle for this site. For stiffer substrates, the elastic reaction force is higher and the dissociation force reaches a higher level (see Eq. A3). Eq. A1, A3, A4 above are combined to provide, using normalized quantities defined from the force (f_β), energy (k_BT), distance (ρ_f) scale indicated above, the self-consistency condition for $\langle F(k)\rangle$:

$$\tilde{F}(\tilde{k}) \approx \ln \tilde{k} + \left[\Delta\tilde{U} + \frac{\Delta\Delta\tilde{U}}{2}\left\{1 + \tanh\left[(\tilde{F}(\tilde{k}) - \tilde{F}_c)\frac{d^*}{\rho_f}\right]\right\}\right] \tag{A7}$$

Fig. 7 summarizes the results obtained for a given dynamic adhesion site (see Results for explanation).

Note that AECs correspond to adhesion sites with the highest maturation (or affinity, i.e., S-values being in the range 0-+1) which means highest dissociation forces. Energy values of such a reinforced link could easily approach 100 $k_B T$, and might correspond to dissociation forces in the range 50-100 pN. Single-bond mechanics of macrophage adhesion via a variety of specific ligands has been done by Knöner et al.(15), leading to a maximum dissociation force of 50 pN at loading rates of 450 pN/s, i.e., 10 pN at 10 pN/s loading rate (see Fig. 11 in (15)), which confirms that AMs adhesion sites have rupture forces markedly smaller than AECs (see Fig. 7).

Acknowledgments

The authors are grateful to the Région d'Ile-de-France for financial support for the AFM equipment acquired by University Paris XII. The authors are also grateful to Professor C. Verdier from CNRS (Grenoble, France) who performed the dynamic tests on gels and who kindly provided the values of viscous losses in polyacrylamide gels. They are also grateful to Patricia Zadigue for cell culture and immunostaining.

References

1. Wong, J. Y., J. B. Leach, and X. Q. Brown. 2004. Balance of chemistry, topography, and mechanics at the cell–biomaterial interface: Issues and challenges for assessing the role of substrate mechanics on cell response. Surface Science 570:119–133.
2. Lo, C. M., H. B. Wang, M. Dembo, and Y. L. Wang. 2000. Cell movement is guided by the rigidity of the substrate. Biophys J 79:144-152.
3. Planus, E., S. Galiacy, M. Matthay, V. Laurent, J. Gavrilovic, G. Murphy, C. Clérici, D. Isabey, C. Lafuma, and M. P. d'Ortho. 1999. Role of collagenase in mediating in vitro alveolar epithelial wound repair. Journal Of Cell Science 112 (Pt 2):243-252.
4. Engler, A. J., M. A. Griffin, S. Sen, C. G. Bonnemann, H. L. Sweeney, and D. E. Discher. 2004. Myotubes differentiate optimally on substrates with tissue-like stiffness: pathological implications for soft or stiff microenvironments. J Cell Biol 166:877-887.
5. Yeung, T., P. C. Georges, L. A. Flanagan, B. Marg, M. Ortiz, M. Funaki, N. Zahir, W. Ming, V. Weaver, and P. A. Janmey. 2005. Effects of substrate stiffness on cell morphology, cytoskeletal structure, and adhesion. Cell Motil Cytoskeleton 60:24-34.
6. Féréol, S., R. Fodil, B. Labat, S. Galiacy, V. M. Laurent, B. Louis, D. Isabey, and E. Planus. 2006. Sensitivity of alveolar macrophages to substrate mechanical and adhesive properties. Cell Motil Cytoskeleton 63:321-340.
7. Gao, M., M. Sotomayor, E. Villa, E. H. Lee, and K. Schulten. 2006. Molecular mechanisms of cellular mechanics. Phys Chem Chem Phys 8:3692-3706.
8. Evans, E. 2001. Probing the relation between force--lifetime--and chemistry in single molecular bonds. Annu Rev Biophys Biomol Struct 30:105-128.
9. Bruinsma, R. F. 2005. Theory of Force Regulation by Nascent Adhesion Sites. Biophys J.
10. Choquet, D., D. P. Felsenfeld, and M. P. Sheetz. 1997. Extracellular matrix rigidity causes strengthening of integrin-cytoskeleton linkages. Cell 88:39-48.

11. Giannone, G., G. Jiang, D. H. Sutton, D. R. Critchley, and M. P. Sheetz. 2003. Talin1 is critical for force-dependent reinforcement of initial integrin-cytoskeleton bonds but not tyrosine kinase activation. J Cell Biol 163:409-419.
12. Galbraith, C. G., K. M. Yamada, and M. P. Sheetz. 2002. The relationship between force and focal complex development. J Cell Biol 159:695-705.
13. Zamir, E., and B. Geiger. 2001. Molecular complexity and dynamics of cell-matrix adhesions. J Cell Sci 114:3583-3590.
14. Block, M. R., C. Badowski, A. Millon-Fremillon, D. Bouvard, A. P. Bouin, E. Faurobert, D. Gerber-Scokaert, E. Planus, and C. Albiges-Rizo. 2008. Podosome-type adhesions and focal adhesions, so alike yet so different. Eur J Cell Biol.
15. Knoner, G., B. E. Rolfe, J. H. Campbell, S. J. Parkin, N. R. Heckenberg, and H. Rubinsztein-Dunlop. 2006. Mechanics of cellular adhesion to artificial artery templates. Biophys J 91:3085-3096.
16. Destaing, O., F. Saltel, J. C. Geminard, P. Jurdic, and F. Bard. 2003. Podosomes display actin turnover and dynamic self-organization in osteoclasts expressing actin-green fluorescent protein. Mol Biol Cell 14:407-416.
17. Collin, O., P. Tracqui, A. Stephanou, Y. Usson, J. Clement-Lacroix, and E. Planus. 2006. Spatiotemporal dynamics of actin-rich adhesion microdomains: influence of substrate flexibility. J Cell Sci 119:1914-1925.
18. Mizuno, D., C. Tardin, C. F. Schmidt, and F. C. Mackintosh. 2007. Nonequilibrium mechanics of active cytoskeletal networks. Science 315:370-373.
19. Alenghat, F. J., S. M. Nauli, R. Kolb, J. Zhou, and D. E. Ingber. 2004. Global cytoskeletal control of mechanotransduction in kidney epithelial cells. Exp Cell Res 301:23-30.
20. Gardel, M. L., F. Nakamura, J. Hartwig, J. C. Crocker, T. P. Stossel, and D. A. Weitz. 2006. Stress-dependent elasticity of composite actin networks as a model for cell behavior. Phys Rev Lett 96:088102.
21. Schaub, S., S. Bohnet, V. M. Laurent, J. J. Meister, and A. B. Verkhovsky. 2007. Comparative maps of motion and assembly of filamentous actin and myosin II in migrating cells. Mol Biol Cell 18:3723-3732.
22. Ingber, D. E. 2003. Tensegrity I. Cell structure and hierarchical systems biology. J Cell Sci 116:1157-1173.
23. Chiquet, M., A. S. Renedo, F. Huber, and M. Fluck. 2003. How do fibroblasts translate mechanical signals into changes in extracellular matrix production? Matrix Biol 22:73-80.
24. Linder, S., and M. Aepfelbacher. 2003. Podosomes: adhesion hot-spots of invasive cells. Trends Cell Biol 13:376-385.
25. Planus, E., S. Galiacy, S. Fereol, R. Fodil, V. M. Laurent, M. P. d'Ortho, and D. Isabey. 2005. Apical rigidity of an epithelial cell monolayer evaluated by magnetic twisting cytometry: ICAM-1 versus integrin linkages to F-actin structure. Clin Hemorheol Microcirc 33:277-291.
26. Pelham, R. J., Jr., and Y. Wang. 1997. Cell locomotion and focal adhesions are regulated by substrate flexibility. Proc Natl Acad Sci U S A 94:13661-13665.
27. Solon, J., I. Levental, K. Sengupta, P. C. Georges, and P. A. Janmey. 2007. Fibroblast adaptation and stiffness matching to soft elastic substrates. Biophys J 93:4453-4461.
28. Laurent, V. M., S. Henon, E. Planus, R. Fodil, M. Balland, D. Isabey, and F. Gallet. 2002. Assessment of mechanical properties of adherent living cells by bead micromanipulation: comparison of magnetic twisting cytometry vs optical tweezers. Journal of Biomechanical Engineering 124:408-421.

29. Wang, N., J. P. Butler, and D. E. Ingber. 1993. Mechanotransduction across the cell surface and through the cytoskeleton [see comments]. Science 260:1124-1127.
30. Ohayon, J., P. Tracqui, R. Fodil, S. Fereol, V. M. Laurent, E. Planus, and D. Isabey. 2004. Analysis of nonlinear responses of adherent epithelial cells probed by magnetic bead twisting: A finite element model based on a homogenization approach. J Biomech Eng 126:685-698.
31. Wendling, S., E. Planus, V. Laurent, L. Barbe, A. Mary, C. Oddou, and D. Isabey. 2000. Role of cellular tone and microenvironmental conditions on cytoskeleton stiffness assessed by tensegrity model. European Physical Journal Applied Physics 9:51-62.
32. Lenormand, G., S. Henon, A. Richert, J. Simeon, and F. Gallet. 2003. Elasticity of the human red blood cell skeleton. Biorheology 40:247-251.
33. Caille, N., O. Thoumine, Y. Tardy, and J. J. Meister. 2002. Contribution of the nucleus to the mechanical properties of endothelial cells. J Biomech 35:177-187.
34. Katoh, K., M. Masuda, Y. Kano, Y. Jinguji, and K. Fujiwara. 1995. Focal adhesion proteins associated with apical stress fibers of human fibroblasts. Cell Motil Cytoskeleton 31:177-195.
35. Tanaka, J., T. Watanabe, N. Nakamura, and K. Sobue. 1993. Morphological and biochemical analyses of contractile proteins (actin, myosin, caldesmon and tropomyosin) in normal and transformed cells. J Cell Sci 104 (Pt 2):595-606.
36. Pourati, J., A. Maniotis, D. Spiegel, J. L. Schaffer, J. P. Butler, J. J. Fredberg, D. E. Ingber, D. Stamenovic, and N. Wang. 1998. Is cytoskeletal tension a major determinant of cell deformability in adherent endothelial cells ? Cell Physiology 43:C1283-C1289.
37. Laurent, V. M., R. Fodil, P. Cañadas, E. Planus, and D. Isabey. 2002. Specific Mechanical and Structural Responses of Cortical and Cytosolic Cytoskeleton in Living Adherent Cells. JSME International Journal (Series C) 45:897-905.
38. Hirata, H., H. Tatsumi, and M. Sokabe. 2007. Dynamics of actin filaments during tension-dependent formation of actin bundles. Biochim Biophys Acta.
39. Li, F., S. D. Redick, H. P. Erickson, and V. T. Moy. 2003. Force measurements of the alpha5beta1 integrin-fibronectin interaction. Biophys J 84:1252-1262.
40. Wang, M., Y. Cao, and H. Li. 2006. The unfolding and folding dynamics of TNfnALL probed by single molecule force-ramp spectroscopy. Polymer 47:2548-2554.
41. Carrion-Vazquez, M., A. F. Oberhauser, S. B. Fowler, P. E. Marszalek, S. E. Broedel, J. Clarke, and J. M. Fernandez. 1999. Mechanical and chemical unfolding of a single protein: a comparison. Proc Natl Acad Sci U S A 96:3694-3699.
42. Wang, N., I. M. Tolic-Norrelykke, J. Chen, S. M. Mijailovich, J. P. Butler, J. J. Fredberg, and D. Stamenovic. 2002. Cell prestress. I. Stiffness and prestress are closely associated in adherent contractile cells. Am J Physiol Cell Physiol 282:C606-616.
43. Stamenovic, D., S. M. Mijailovich, I. M. Tolic-Norrelykke, J. Chen, and N. Wang. 2002. Cell prestress. II. Contribution of microtubules. Am J Physiol Cell Physiol 282:C617-624.
44. Cañadas, P., V. M. Laurent, C. Oddou, D. Isabey, and S. Wendling. 2002. A Cellular Tensegrity Model to Analyse the Structural Viscoelasticity of the Cytoskeleton. J Theor Biol 218:155-173.
45. Takagi, J., B. M. Petre, T. Walz, and T. A. Springer. 2002. Global conformational rearrangements in integrin extracellular domains in outside-in and inside-out signaling. Cell 110:599-511.
46. Engler, A., L. Bacakova, C. Newman, A. Hategan, M. Griffin, and D. Discher. 2004. Substrate compliance versus ligand density in cell on gel responses. Biophys J 86:617-628.

47. Zaman, M. H., R. D. Kamm, P. Matsudaira, and D. A. Lauffenburger. 2005. Computational model for cell migration in three-dimensional matrices. Biophys J 89:1389-1397.
48. Schwarz, U. S., T. Erdmann, and I. B. Bischofs. 2006. Focal adhesions as mechanosensors: the two-spring model. Biosystems 83:225-232.
49. Jiang, G., G. Giannone, D. R. Critchley, E. Fukumoto, and M. P. Sheetz. 2003. Two-piconewton slip bond between fibronectin and the cytoskeleton depends on talin. Nature 424:334-337.
50. Thoumine, O., A. Ott, and D. Louvard. 1996. Critical centrifugal forces induce adhesion rupture or structural reorganization in cultured cells. Cell Motil Cytoskeleton 33:276-287.
51. Zamir, E., M. Katz, Y. Posen, N. Erez, K. M. Yamada, B. Z. Katz, S. Lin, D. C. Lin, A. Bershadsky, Z. Kam, and B. Geiger. 2000. Dynamics and segregation of cell-matrix adhesions in cultured fibroblasts. Nat Cell Biol 2:191-196.
52. Geiger, B., and A. Bershadsky. 2001. Assembly and mechanosensory function of focal contacts. Curr Opin Cell Biol 13:584-592.
53. Wang, N., and Z. Suo. 2005. Long-distance propagation of forces in a cell. Biochem Biophys Res Commun 328:1133-1138.
54. Cai, S., L. Pestic-Dragovich, M. E. O'Donnell, N. Wang, D. Ingber, E. Elson, and P. De Lanerolle. 1998. Regulation of cytoskeletal mechanics and cell growth by myosin light chain phosphorylation. Am J Physiol 275:C1349-1356.
55. Balland, M., A. Richert, and F. Gallet. 2005. The dissipative contribution of myosin II in the cytoskeleton dynamics of myoblasts. Eur Biophys J 34:255-261.
56. Wendling, S., C. Oddou, and D. Isabey. 1999. Stiffening response of a cellular tensegrity model. Journal Of Theoretical Biology 196:309-325.
57. Balaban, N. Q., U. S. Schwarz, D. Riveline, P. Goichberg, G. Tzur, I. Sabanay, D. Mahalu, S. Safran, A. Bershadsky, L. Addadi, and B. Geiger. 2001. Force and focal adhesion assembly: a close relationship studied using elastic micropatterned substrates. Nat Cell Biol 3:466-472.
58. Riveline, D., E. Zamir, N. Q. Balaban, U. S. Schwarz, T. Ishizaki, S. Narumiya, Z. Kam, B. Geiger, and A. D. Bershadsky. 2001. Focal contacts as mechanosensors: externally applied local mechanical force induces growth of focal contacts by an mDia1-dependent and ROCK-independent mechanism. J Cell Biol 153:1175-1186.
59. Icard-Arcizet, D., O. Cardoso, A. Richert, and S. Henon. 2008. Cell stiffening in response to external stress is correlated to actin recruitment. Biophys J 94:2906-2913.
60. Ridley, A. J., and A. Hall. 1992. The small GTP-binding protein rho regulates the assembly of focal adhesions and actin stress fibers in response to growth factors. Cell 70:389-399.
61. Besser, A., and U. S. Schwarz. 2007. Coupling biochemistry and mechanics in cell adhesion: a model for inhomogeneous stress fiber contraction. New Journal of Physics 9:425.
62. Jones, G. E., W. E. Allen, and A. J. Ridley. 1998. The Rho GTPases in macrophage motility and chemotaxis. Cell Adhes Commun 6:237-245.
63. Ridley, A. J. 2008. Regulation of macrophage adhesion and migration by Rho GTP-binding proteins. J Microsc 231:518-523.
64. Evans, E., A. Leung, and D. Zhelev. 1993. Synchrony of cell spreading and contraction force as phagocytes engulf large pathogens. J Cell Biol 122:1295-1300.
65. Beningo, K. A., and Y. L. Wang. 2002. Fc-receptor-mediated phagocytosis is regulated by mechanical properties of the target. J Cell Sci 115:849-856.
66. Ingber, D. E. 2003. Tensegrity II. How structural networks influence cellular information processing networks. J Cell Sci 116:1397-1408.

67. Burgstaller, G., and M. Gimona. 2004. Actin cytoskeleton remodelling via local inhibition of contractility at discrete microdomains. J Cell Sci 117:223-231.

Legend of figures

Figure 1:
a and b: cumulative views of F-actin and paxillin in fixed AECs (a) and AMs (b) adhering on the same type I collagen-coated glass substrates. These images were made of z-stack of confocal images within a 1µm-thick layer from the basal cell plane.
c and d: Top view of 3D-skeletonization and 3D-reconstructions of the aggregated paxillin obtained in the same AECs (c) and AMs (d) from the images shown in a and b.
e and f: Side view of 3D-skeletonization and 3D-reconstructions of the aggregated paxillin obtained in the same AECs (e and AMs (f) from the images shown in a and b.

Figure 2: The CSK elastic modulus (in Pa) or stiffness of alveolar epithelial cells (AECs) and alveolar macrophages (AMs) is measured by RGD-coated ferromagnetic beads (~ 4.5 µm in diameter) using the Magnetic Twisting Cytometry (MTC) technique for four different magnetic torques in the range 230 pN·µm – 1300 pN·µm. There is a highly significant increase in CSK elastic modulus with magnetic torque for AECs (stress hardening cell response) and an almost constant CSK elastic modulus with stress increase (stress independent cell response). Values are expressed a mean ± s.e.m.. Each value is the mean of three independent measurements. The statistical test used here is the Anova test. (* $p<0.05$; *** $p<0.001$)

Figure 3: The magnetic torque (in pN·µm) is plotted versus the bead rotation angle (in degrees) or its equivalent in terms of bead displacement (in nm) calculated at the surface of a 4.5 µm diameter bead, for alveolar epithelial cells (AECs) and alveolar macrophages (AMs). MTC measurements correspond to an intermediate to large range of cellular deformations (from 500 nm to 2000 nm). Note that the Optical Tweezers Method used here (see Methods) operate over the range of small cellular deformation (28). We postulate that cell breakage might occur in the highest range of cell deformations. Values are expressed as mean ± s.e.m.. Each value is the mean of three independent measurements. The statistical test used here is the Anova test (*** $p<0.001$).

Figure 4: The CSK elastic modulus (in Pa) of alveolar epithelial cells (AECs) and alveolar macrophages (AMs) in the 11 minutes following an actin-depolymerising treatment with cytochalasin D. Measurements were performed with MTC. Slight differences in absolute values of AMs elastic modulus found with Fig. 1 remain in the statistical range of error. As previously shown (31), the decay in CSK elastic modulus during cytochalasin D treatment can be related to prestress. Values are expressed as mean ± s.e.m.. Each value is the mean of three independent measurements. The statistical test used here is the Anova test (***: $p < 0.001$).

Fig. 5: The effect of substrate stiffness on F-actin structures and CSK elastic modulus (in Pa) is shown in A for alveolar epithelial cells (AECs) and B for alveolar macrophages (AMs). Three type I collagen-coated substrates of different stiffness values were tested, i.e., successively from left to right in A and B: plastic/glass substrate (E_S (Young modulus) ≥ 3

MPa); stiff gel (E_S = 58 kPa); soft gel (E_S = 23 kPa). Images A1 to A6 provide for AECs and B1 to B6 for AMs, 3D-visualizations of F-actin structure from cumulated images of confocal planes viewed from top (A1 to A3 and B1 to B3) and from the side (A4 to A6 and B4 to B6). Graphs on bottom of A and B represent respectively the elastic modulus (in Pa) of confluent AECs (measured through RGD-coated ferromagnetic beads by MTC) and resting AMs (measured through RGD-coated silicate beads by OT) plotted for the three different substrates tested. Note that different scales are used in A and B. Values are expressed as mean ± s.e.m.. Each value is the mean of three independent measurements. The statistical test used here is the Anova test. No significant differences were observed in AECs.

Fig. 6: 3D-stress fields calculated by numerical simulation for the three substrates tested in the experimental study: (a) rigid plastic substrate (3000 kPa), (b) stiff gel (58 kPa) and (c) soft gel (23 kPa). The planar cross-sectional views of the 3D-stress field are obtained for a constant magnetic torque (namely 750 nN·µm) applied by a partially immersed bead (4.5 µm in diameter, 130° of half angle of bead immersion) in an isolated cell of constant Young modulus property (100 Pa) continuously attached to the three substrates tested. This numerical simulation assumes linearly elastic materials, continuity conditions at the cell-substrate interface and static equilibrium between bead, cell and substrate. Note that, in spite of very different stiffness properties of the substrate, the stress field “seen” at the cell-substrate interface is the same for the three very different substrates studied. This simulation is a new demonstration that the stress-distribution of an elastic medium subject to a localized external force exerted on the surface does not depend on the stiffness of the medium.

Fig. 7: The normalized most likely dissociation force $\tilde{F}(\tilde{k})$ for a given adhesion site is plotted versus the normalized substrate stiffness $\tilde{k}$ (given by Eq. A5). The values of the state parameter S increase from −1 to +1 as the energy level required for adhesion site dissociation increases. S ~ −1 corresponds to the lowest level of dissociation energy ($\Delta\tilde{U}$) and thus to a fully slipping adhesion site. AM adhesion sites would correspond to an intermediate range of S values (−1; 0) corresponding to the transition between logarithmic dependence and the increasing contribution of elastic energy associated to the displacement (i.e., $0.5\, k\left(\rho - V_R\, t\right)^2$). In this zone, the adhesion site is in a dynamic state and substrate-dependent changes are reversible. Beyond a critical value of substrate rigidity $\tilde{k}_c$ is difficult to more precisely determine at the present time (see Appendix), the adhesion site is reinforced and fully transmits the actomyosin traction force to the substrate. Adhesion sites of AECs pertain to this zone (S values in the range (0; +1) in which adhesion sites are stationary and irreversibly reinforced. The highest level of dissociation energy $\Delta\Delta\tilde{U}$ is observed for S~ +1

Fig. 8: Synthetic diagram predicting the variation in the cellular sensitivity to substrate stiffness as a function of two determinant parameters plotted on the two horizontal axis: (i) adhesion force reflecting the state of adhesion sites, and (ii) CSK prestress reflecting actomyosin contractility. The adhesion strength increases as adhesion site is reinforced: pN range for Initial Adhesion (IA), nN range for premature Focal Complex (FC) and µN range for mature Focal Adhesion (FA). Podosome Type Adhesion (PTA) characterizing macrophage adhesion is right in between IA and FC in terms of adhesion site strength and dynamic state. Adhesion site contractility is susceptible to change from local scale, e.g., in podosomes (PTA), to global scale, e.g., in stress fiber network, the intermediate situation for prestress corresponding to actomyosin contractility in lamellipodia, also responsible for actin retrograde velocity. This diagram is consistent with both the theory (described in Appendix)

and the experiments. Confluent TC (tissue cells) such as AECs in monolayer are usually highly stressed cells with a fairly stationary focal adhesion system. They exhibit almost no sensitivity to substrate stiffness as predicted by the stationary adhesion site theory. When isolated, TC can express dynamic adhesion sites and recover their sensitivity to substrate stiffness. Resting AMs with low or intermediate internal stress and essentially dynamic adhesion sites exhibit a net sensitivity to substrate stiffness. The diagram predicts that unstressed cells with essentially fully slipping adhesion sites cultured on very soft substrates would lack sensitivity to substrate stiffness.

Fig. A1: Schema of the dynamic adhesion site model.

The dynamic adhesion site model takes into account the chemico-physical link: cytoskeleton, adhesion site and extracellular matrix (ECM), and the associated forces and mechanical properties. The adhesion site and the actin bundle can move along the axis direction x under the action of constant traction T exerted on actin bundle and the viscoelastic recoil exerted by the substrate on the adhesion site. The relative distance between the adhesion site and the actin bundle is called $\rho(t)$. The link between adhesion site and actin filament bundle is described by a “two state” potential energy of mean force whose state varies between passive (S=-1) and active (S=+1) (see Fig. 7). This mechano-chemical reaction is assumed to involve conformational change of the adhesion site integrins. (see text for explanations).

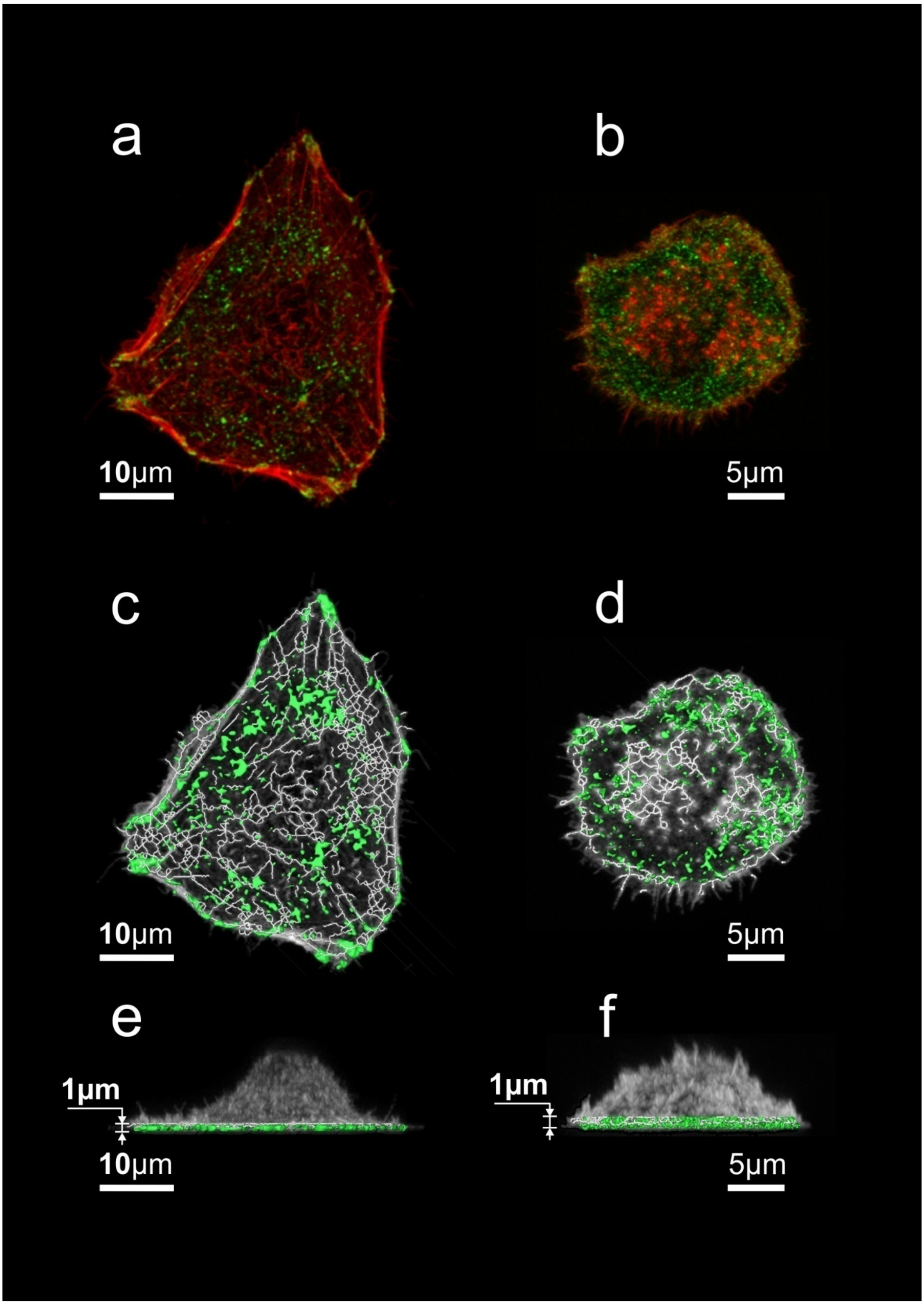

Figure 1

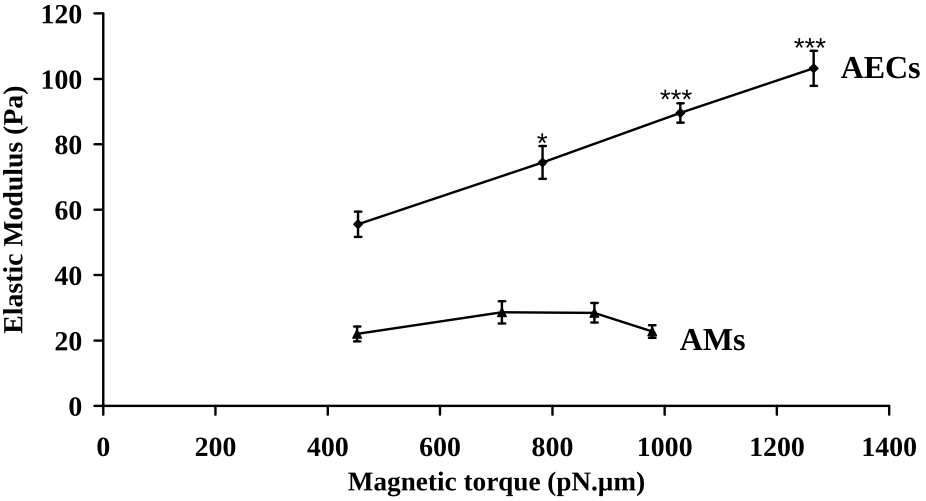

Figure 2

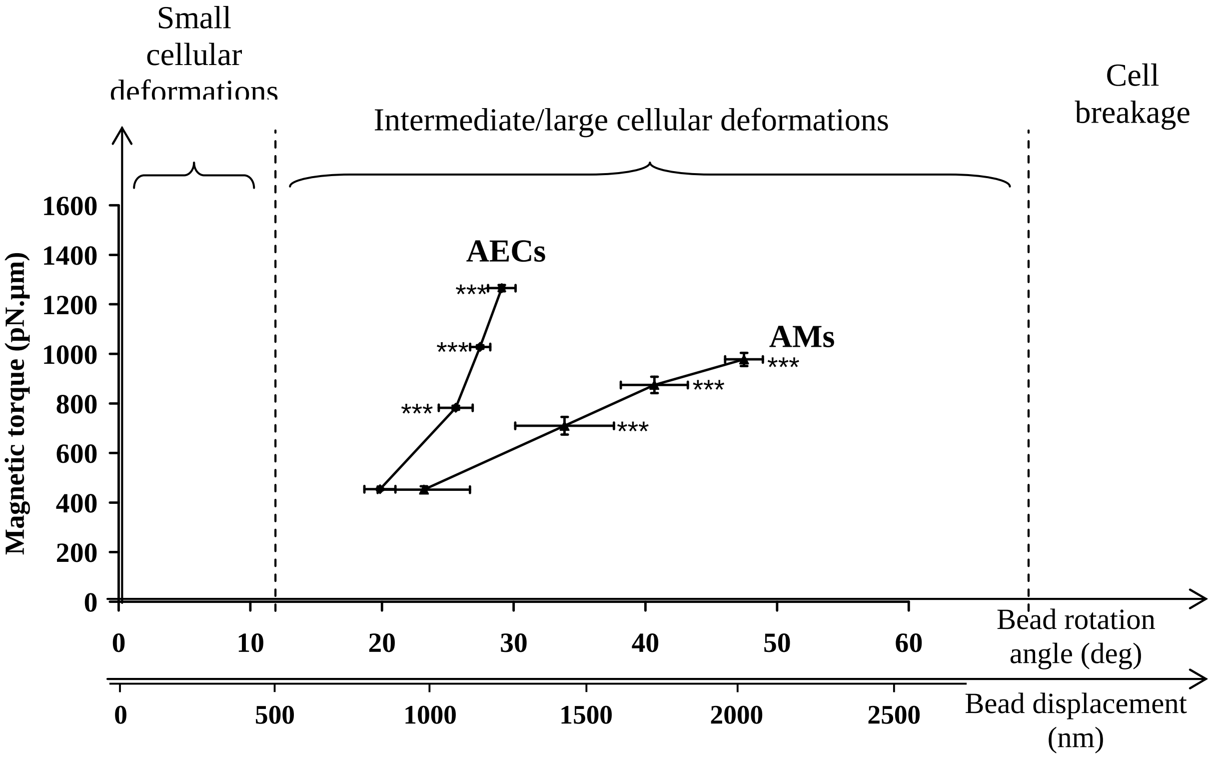

Figure 3

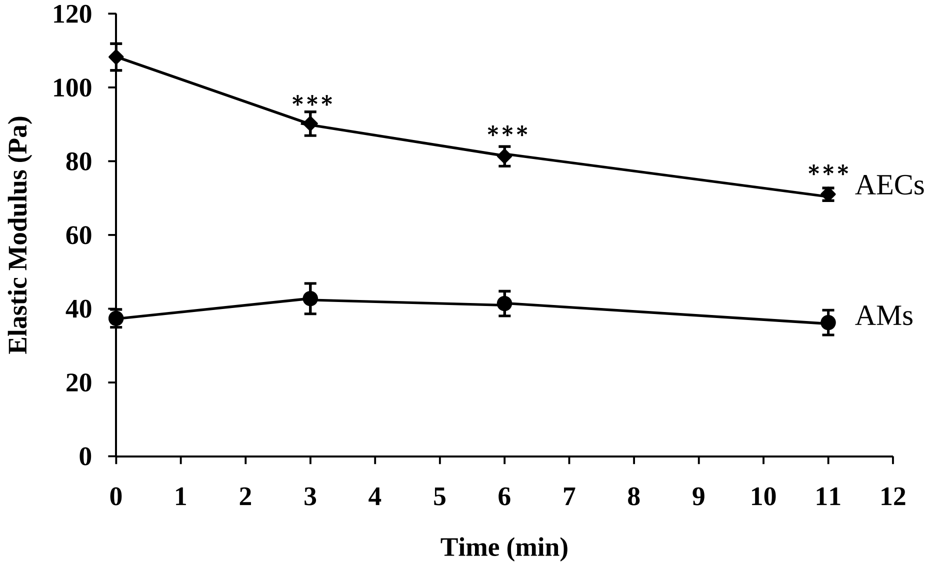

Figure 4

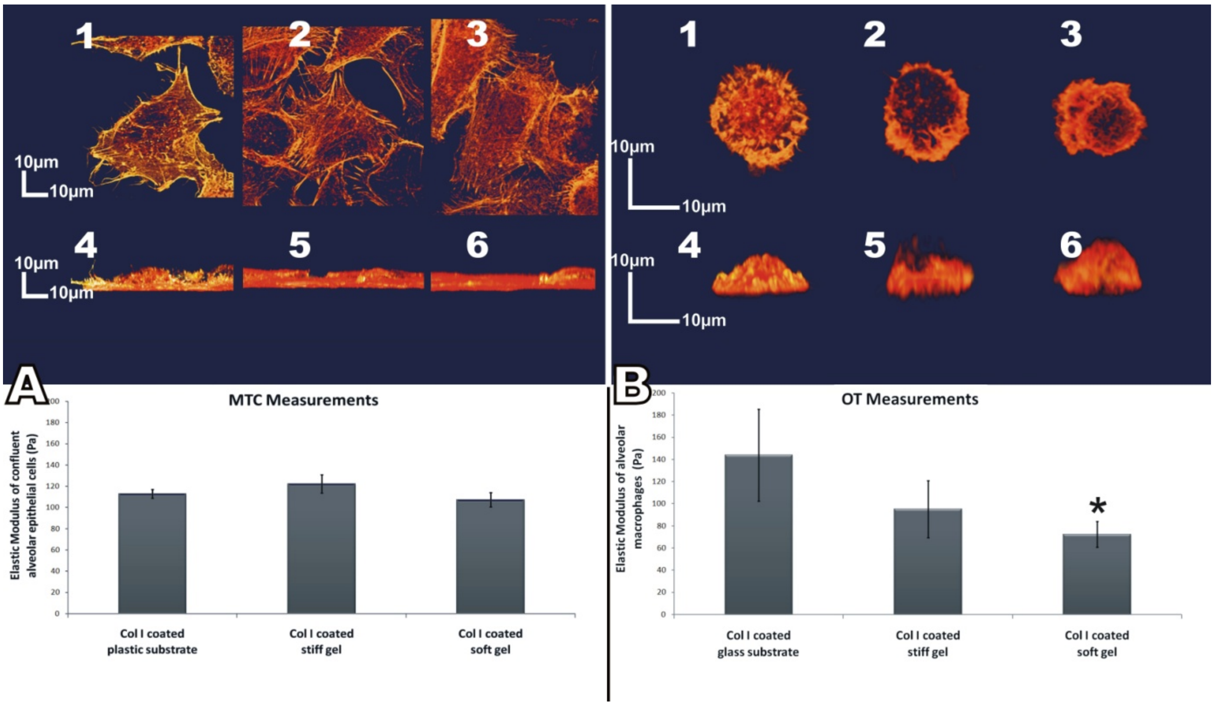

Figure 5

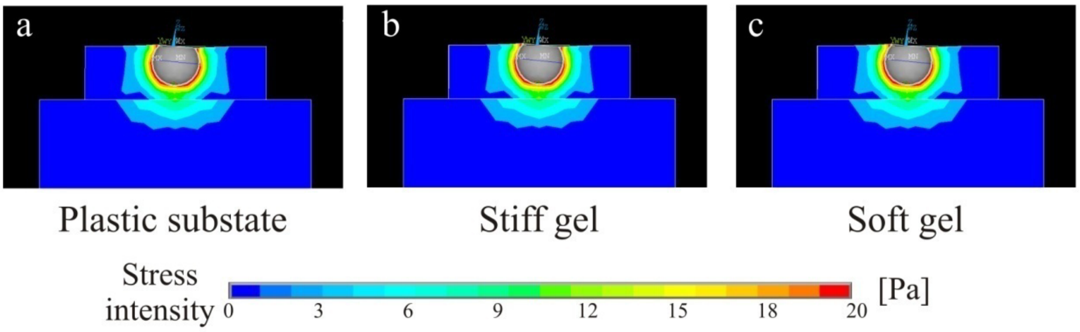

Figure 6

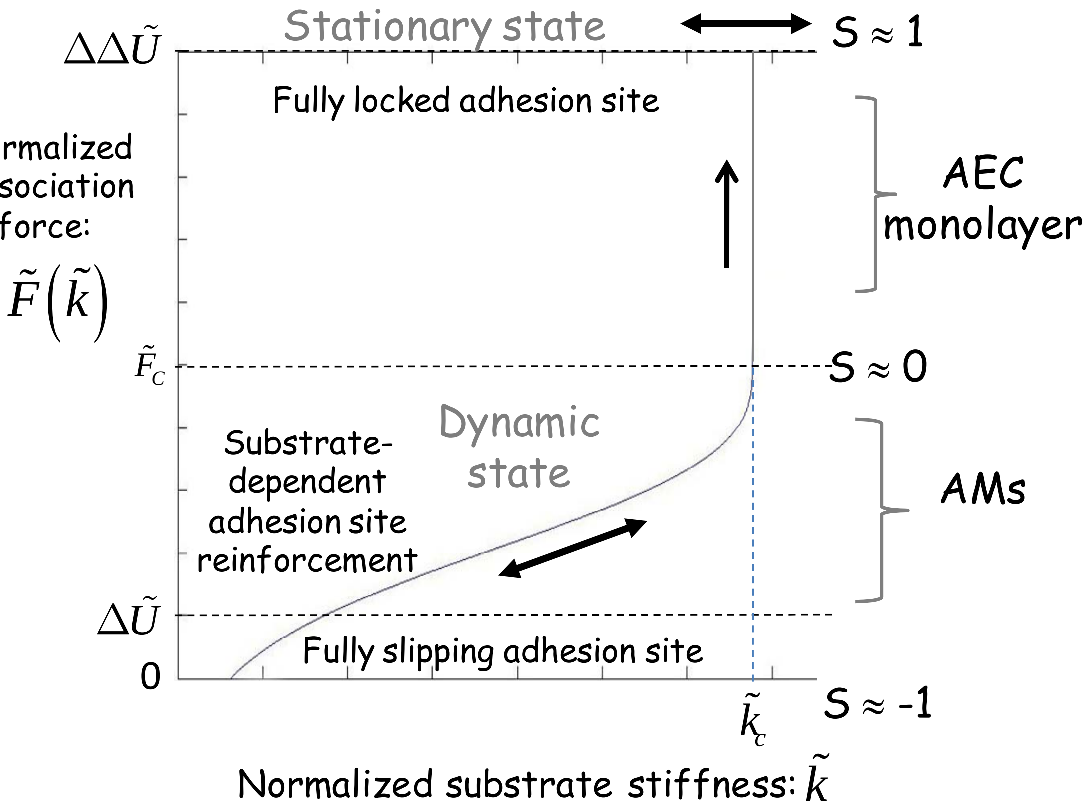

Figure 7

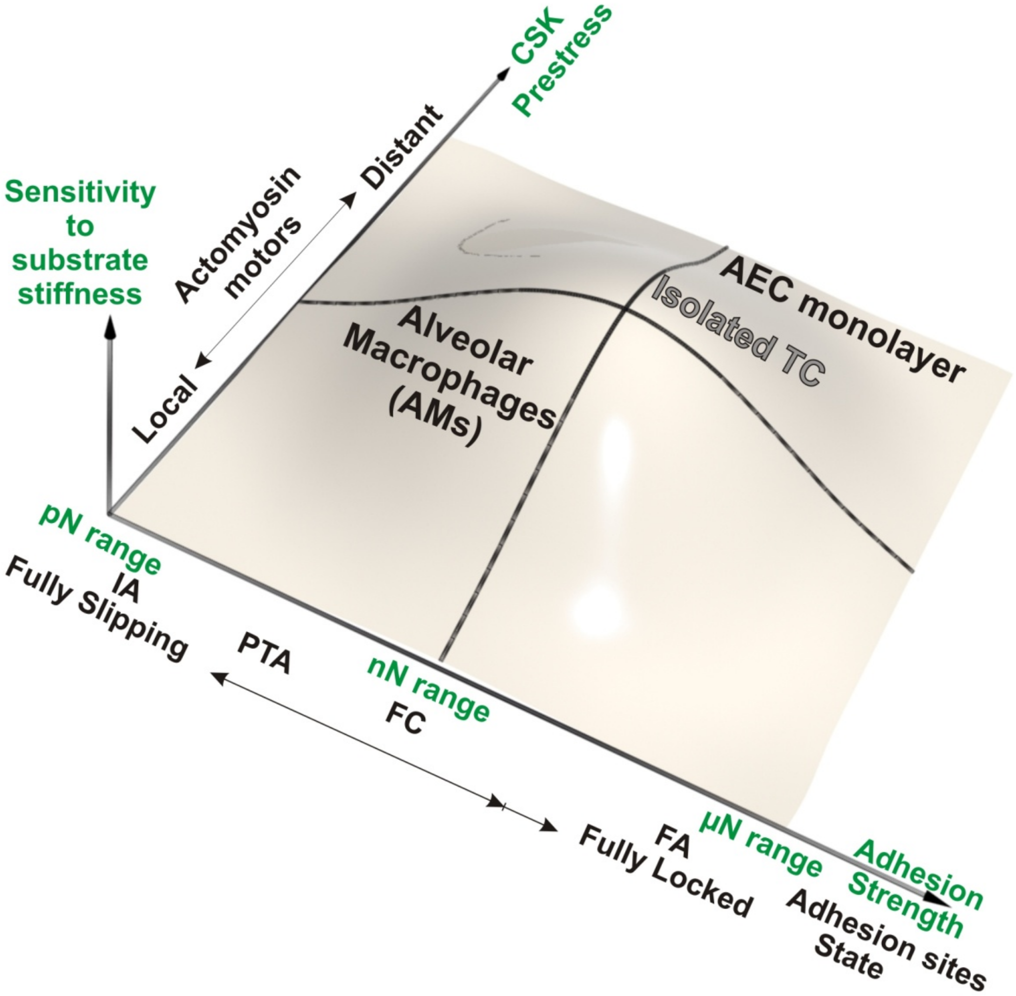
CSK Prestress
Distant
Actomyosin motors
Local
Sensitivity to substrate stiffness
AEC monolayer
Isolated TC
Alveolar Macrophages (AMs)
pN range
IA
Fully Slipping
PTA
nN range
FC
µN range
FA
Fully Locked
Adhesion Strength
Adhesion sites State

Figure 8

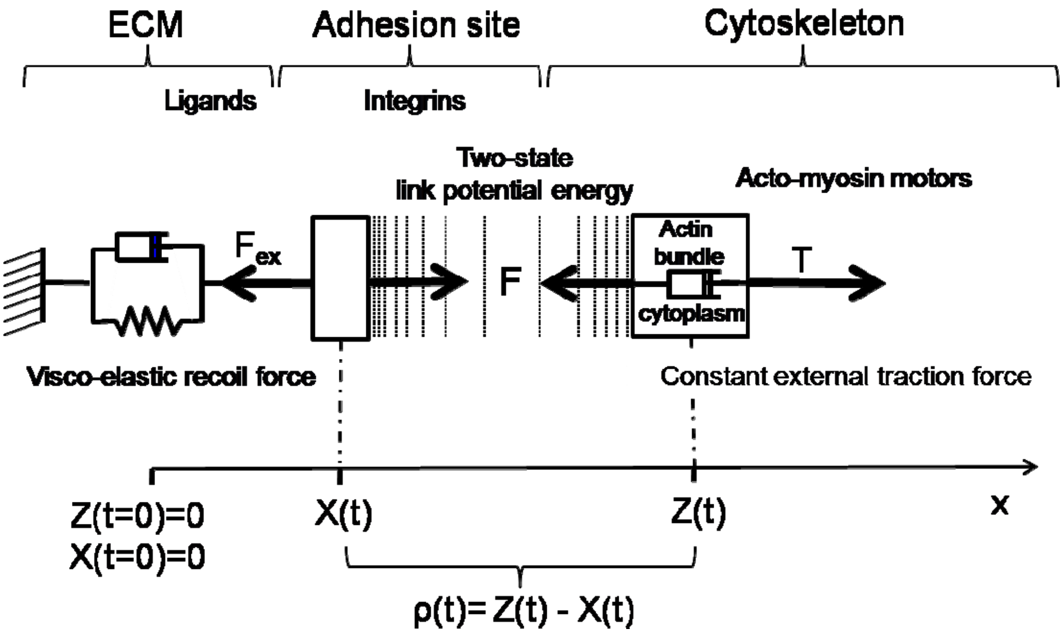
ECM
Adhesion site
Cytoskeleton
Ligands
Integrins
Two-state
link potential energy
Acto-myosin motors
F_{ex}
F
Actin
bundle
cytoplasm
T
Visco-elastic recoil force
Constant external traction force
Z(t=0)=0
X(t=0)=0
X(t)
Z(t)
x
ρ(t)= Z(t) - X(t)

Figure A1